ShakeOut Scenario Appendix C: Characteristics of Earthquake-Induced Permanent Ground Deformation and Examples from Past Earthquakes

By John Tinsley III[1] and Daniel Ponti[1]

USGS Open File Report 2008-1150, Appendix C
CGS Preliminary Report 25C

2008

U.S. Department of the Interior
U.S. Geological Survey

California Department of Conservation
California Geological Survey

[1] **U.S. Geological Survey**

U.S. Department of the Interior
DIRK KEMPTHORNE, Secretary

U.S. Geological Survey
Mark D. Myers, Director

State of California
ARNOLD SCHWARZENEGGER, Governor

The Resources Agency
MIKE CHRISMAN, Secretary for Resources

Department of Conservation
Bridgett Luther, Director

California Geological Survey
John G. Parrish, Ph.D., State Geologist

U.S. Geological Survey, Reston, Virginia 2008

For product and ordering information:
World Wide Web: http://www.usgs.gov/pubprod
Telephone: 1-888-ASK-USGS

For more information on the USGS—the Federal source for science about the Earth, its natural and living resources, natural hazards, and the environment: World Wide Web: http://www.usgs.gov
Telephone: 1-888-ASK-USGS

Suggested citation:
Tinsley, John, III, and Ponti, Daniel, 2008, ShakeOut Scenario Appendix C; Characteristics of earthquake-induced permanent ground deformation and examples from past earthquakes, Appendix C *of* Jones, L.M., and others, The ShakeOut Scenario: U.S. Geological Survey Open-File Report 2008-1150, and California Geological Survey Preliminary Report 25C, 33 p.
[http://pubs.usgs.gov/of/2008/1150/appendixes/of2008-1150_appendix_c.pdf].

ShakeOut Scenario

Appendix C. Characteristics of Earthquake-Induced Permanent Ground Deformation and Examples from Past Earthquakes

by John Tinsley III and Daniel Ponti, USGS

Primary surface faulting along the trace of the San Andreas fault between the Salton Sea and Lake Hughes, and ground failure resulting from liquefaction and landsliding, are the primary types of permanent ground deformation that we expect will result from the M_w 7.8 ShakeOut Scenario earthquake. The processes controlling these phenomena are well enough understood that the expected locations and displacement magnitudes can be reasonably estimated, assuming that sufficient information about local conditions is known. Here we describe the general characteristics and controls on the types of ground deformation features that we expect to occur from the Scenario event.

Primary Surface Faulting

Many of the physical characteristics of the earth's surface are largely derived from plate tectonics, where a brittle upper crust rides atop a ductile and deforming lower crust and mantle. These interactions produce the blocks of uplifted, down-dropped, tilted, and/or folded crust separated by faults that yield our earth's primary topography (Molnar, 1988; Spotila and others, 2007). This deformation occurs at scales ranging from localized shearing of rocks observable only under the microscope, to patterns of regional deformation that make up California's principal landscape elements, including the Transverse Ranges, the Sierra Nevada mountains, the Great Valley of California, the Coast Ranges, and the Salton trough, to identify a few of California's geomorphic provinces that result from plate tectonic processes and effects.

California has many physiographic examples of the effects of plate tectonics. However, the centerpiece is the San Andreas fault, which forms an active transform boundary where the North American plate moves southeastward relative to the Pacific crustal plate. The San Andreas fault extends from the Salton Sea in the south to the Mendocino Escarpment in the north. The San Andreas and its related faults provide California with many of its damaging earthquakes.

Even though the San Andreas hasn't ruptured in southern California since 1857, careful observations of the 1906 earthquake (which occurred on the San Andreas fault in northern California) and studies of major transform fault earthquakes elsewhere in the world, have provided numerous examples of what the surface rupture of a great southern San Andreas fault earthquake will likely look like.

On November 3, 2002, a M_w 7.9 earthquake ruptured a 300-km section of the Denali fault in southeastern Alaska, locally producing more than 8 meters of right-lateral displacement. In terms of fault rupture length and surface fault displacement, the Denali earthquake is very similar to the ShakeOut scenario event and, along with other examples of strike-slip earthquakes, serves as a useful analog for evaluating surface faulting effects. For most of its length, the observed Denali earthquake's surface rupture was about 1 to 4 meters wide, a remarkably narrow zone (see Figures

A1-1 through A1-3); furthermore, the rupture occurred along pre-existing traces of the fault as evidenced in the geomorphology. Terraces, ridges, swales and similar small-scale features of the topography are evidence that surface faulting occurs repeatedly at or near the same location from one earthquake to the next.

Figure A1-1. The remarkably narrow surface rupture of the Denali fault about 184 km east of the epicenter is shown as it traverses a formerly glaciated valley. Photograph by David P. Schwartz, U. S. Geological Survey.

Figure A1-2: A U.S. Geological Survey field worker straddles the entire width of the Denali earthquake rupture near km 184, thus emphasizing the generally narrow width of such features, despite large right-lateral displacements amounting to several meters. Photograph by David P. Schwartz, U. S. Geological Survey.

Figure A1-3. Primary surface faulting produced by the M_w 7.9 Denali Fault Earthquake of November 3, 2002. The Denali fault trace traverses left to right in the middle ground where the margin of an unvegetated stream channel is offset a distance of 8.1 meters. Without special engineering, any road, pipeline, or structure that crossed the fault here would be severed and offset by that amount. Measurements of the amount of separation of geomorphic features such as this one provide earth scientists with data indicating how surface displacement varies along a given fault rupture. (Photograph by David P. Schwartz, USGS.)

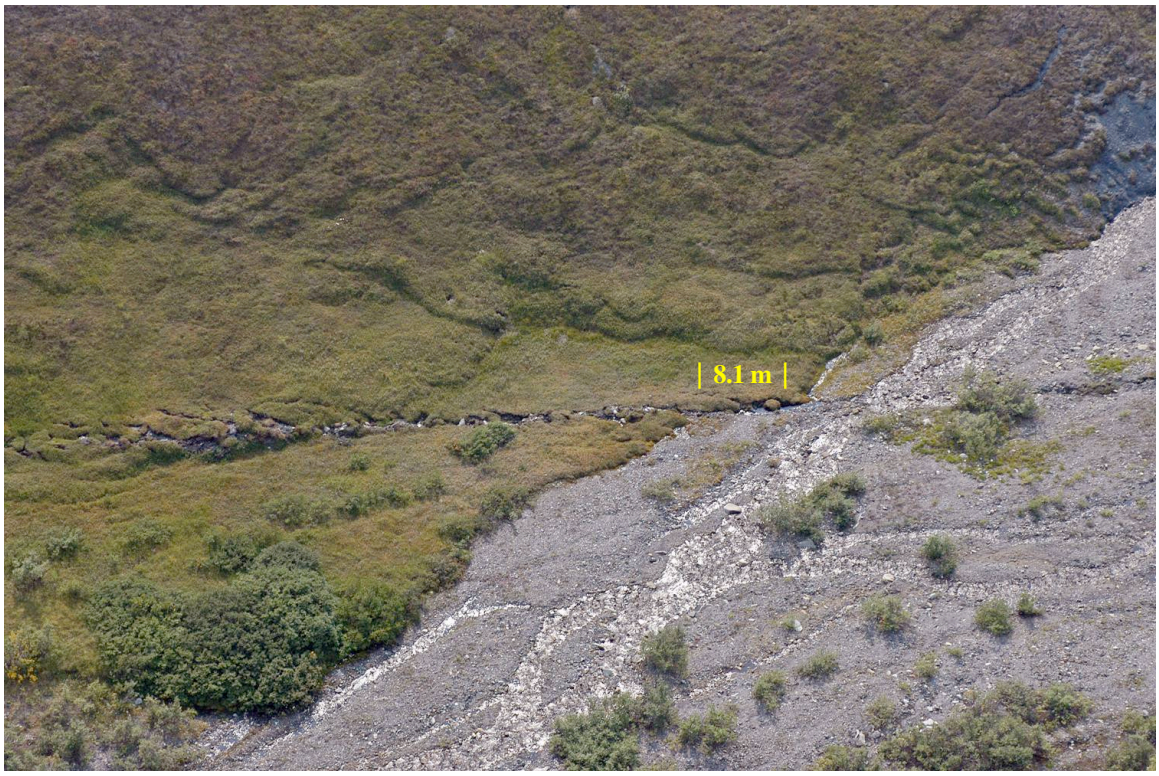

Although the surface rupture of a great earthquake may be relatively narrow along much of its length, and thus of limited extent in terms of its effects on the built environment, faults are not perfectly straight features and there may be more than one surface rupture trace, owing to geological complexities within and near the fault zone. Along strike-slip faults such as the San Andreas fault, the pattern of faulting tends to be simple where the displacement is parallel to the fault trace, but more complex where the fault bends and therefore parts of the fault surface are in compression or tension. This is illustrated in Figure A1-4 where a generally north-trending right-lateral strike-slip fault that curves to the west forms a *restraining bend*, whereas a north-trending right-lateral strike-slip fault that curves to the east forms a *releasing bend*. Compressional features are developed in restraining bends, including reverse faults, pressure ridges, and folding. Extensional features are developed in releasing bends, including graben, topographic low areas such as sag ponds, and localized zones of normal faulting. More than one surface fault trace is commonly observed in both restraining and releasing bends. In addition, where faults traverse areas underlain by relatively thick unconsolidated deposits or encounter a contrast in materials along their trend, the pattern of surface fractures that develops may become more complex (Figure A1-5). Acharya (1997) provides a useful discussion of the influence of fault bends on ruptures at regional scales with respect to the San Andreas fault in southern California.

Figure A1-4. Two generally north-trending right lateral strike-slip faults are diagrammed to illustrate restraining versus releasing bends. Fault A bends to the west at its north end before returning to its northward trend; fault B bends to the east at its north end before returning to its northward trend. As a consequence of San Andreas-like right-lateral displacement, Fault A will develop compressional deformation features along the restraining bend. Fault B will develop extensional features near its releasing bend. Large dark arrows show principal strain direction; light arrows show localized stresses generated owing to changes in the trend of the faults relative to the principal strain direction.

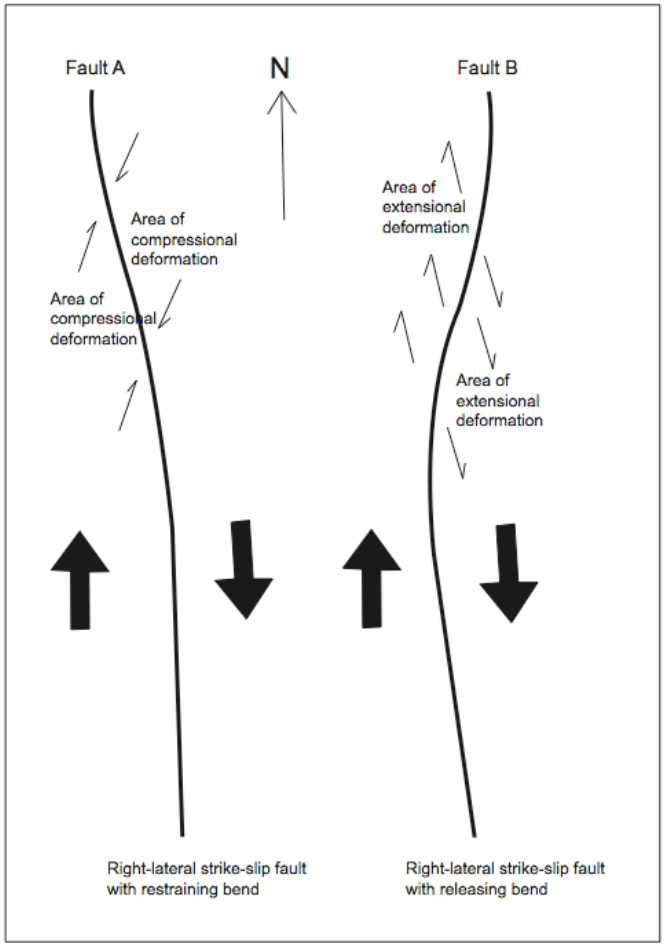

Figure A1-5. A faulted playa lies within a broad releasing bend of the 1992 M_w 7.3 Landers earthquake fault rupture zone, which traverses from the lower left to upper right of the photo. The playa deposits have accumulated in a depression adjacent to a relatively uplifted alluvial surface (grey, dissected) that formed from repeated displacement along the fault in past earthquakes. Several closely spaced surface traces of the Landers earthquake fault rupture increase in number and broaden as they traverse the playa. The fine-grained, brittle nature of the playa deposits serves to better record the complex nature of faulting at this locality. Photograph by Michael J. Rymer, U. S. Geological Survey.

Where strike-slip fault displacement at the surface amounts to 1 meter or less, such as measured along the San Andreas fault from the Parkfield earthquake of 2004 (Rymer and others, 2006) or along the Motagua fault that produced the M_w 7.5 Guatemala earthquake of 1976 (Espinosa, 1976), surface rupture is often expressed as discontinuous en echelon fissures that define a zone of surface faulting a few meters wide; at larger displacements, these fissures may locally coalesce to form a "mole track" representative of more continuous rupture (Figure A1-6). Although modeled fault slip is generally large throughout much of the inferred ShakeOut rupture zone, fissuring and mole tracks are likely to form near the ends of the rupture and on secondary strands within the fault zone that carry only a portion of the total slip.

Figure A1-6. A "mole track" along the trace of the Motagua fault, produced from the 1976 Guatemala earthquake, crosses a soccer field at Gualan. Displacement at this locality is 93 cm left-lateral. Note the right-stepping en echelon fissures and connecting pressure ridges that are characteristic of strike-slip displacement. As displacements decrease, discontinuous en echelon fissures remain. Portions of the ShakeOut fault rupture with lower displacements will likely have similar expression, only the en echelon fissures will "step left" - a result of right-lateral fault displacement. Photograph from the U.S. Geological Survey Photographic Library (ID: Earthquake Information Bulletin 94)

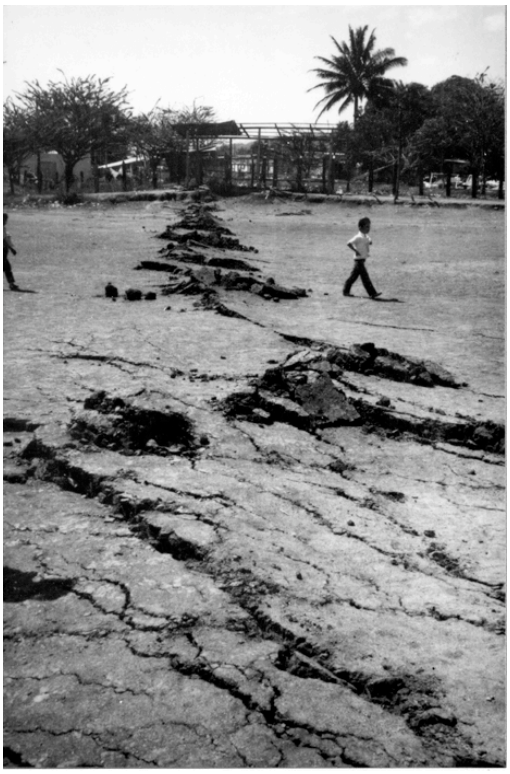

When faults break the ground surface during earthquakes, large displacements can cause extensive damage to structures and lifelines that may be built across them (Figure A1-7). However, the number of structures affected by surface faulting is extremely small compared to the number of buildings that are damaged from strong ground motion across a region.

Figure A1-7. Examples of damage from surface faulting to structures and crossing lifelines. *a)* Wood frame house sheared due to faulting from the 1992 Landers earthquake. The building rotated over the fault rupture (arrow), causing the structure to rip apart several meters away. Although the building did not collapse, it was a total loss. Photograph by Michael J. Rymer, U. S. Geological Survey. *b)* Railroad rails at Puerto Barrios, bent and displaced due to faulting from the 1976 Guatemala earthquake (Fig. 42C from Espinosa, 1976).

a)

b)

Specific effects of fault rupture to structures or buried utilities depend on both the amount of fault slip and the orientation of the fault trace relative to the man-made features. Depending on this relationship,

man-made structures may be stretched or shortened by the faulting in addition to being sheared (see Figure A1-8).

Figure A1-8. Fault displacement from the M_w 7.3 1992 Landers earthquake crosses the chain-link fence in this photograph at an oblique angle (from upper left to lower right) producing compression and causing the fence to shorten, which is expressed by buckling and formation of the S-shaped folds. Depending on how structures are oriented across a fault trace, damage can result from compression or extension, in addition to shearing. Photograph by Michael J. Rymer, U. S. Geological Survey.

We can infer from past earthquakes that faulting from the ShakeOut scenario event will most likely occur along pre-existing surface traces of the San Andreas fault, as evidenced in the geomorphology. Where the fault is straight and simple in form, the rupture will be expressed dominantly as right-lateral horizontal displacement within a zone only a few meters wide. In areas where the fault surface geometry is more complex, such as the San Gorgonio Pass area and locally elsewhere along the fault zone where multiple fault traces have been mapped, faulting may become more complex and occur across a much broader zone. Although few structures are built across the fault within the ShakeOut rupture zone, those that are will likely experience significant damage. Roads and lifelines that cross the fault rupture will also be damaged; the nature and degree of this damage is dependent upon both the amount of fault displacement and the orientation of the faulting relative to the crossing lifelines.

Liquefaction

Youd (1973, p. 1) defined liquefaction as “the transformation of a granular material from a solid state into a liquefied state as a consequence of increased pore-water pressures” that are produced by strong ground shaking. As a result of this transformation, formerly solid ground is transformed temporarily

to a softened or liquefied state that can no longer support the built environment. Effects of liquefaction commonly are observed following moderate to great earthquakes throughout the world. Research addressing the process, occurrence, and consequences of liquefaction was stimulated chiefly by the catastrophic ground failures generated by the 1964 Good Friday Alaska earthquake (Hansen, 1965; McCulloch and Bonilla, 1970) and the 1964 Niigata, Japan, earthquake (Seed and Idriss, 1970). Noteworthy subsequent earthquakes that also stimulated research towards understanding the liquefaction phenomenon include the 1967 Caracas, Venezuela, earthquake (Seed and Alonso, 1973), the 1971 San Fernando (Sylmar) earthquake (Youd, 1971; Seed and others, 1975), the 1979 and 1981 Imperial Valley earthquakes (Johnson and others, 1982; Sharp and others, 1986), the 1989 Loma Prieta, California, earthquake (Holzer, 1998), and the 1994 Northridge, California, earthquake (Holzer et al, 1999). These studies among many others have firmly linked liquefaction to a suite of hydrologic and geologic conditions such that liquefaction as a process is now relatively well understood. The environments that favor the occurrence of liquefaction can be delineated with reasonable precision and the geographic variation in liquefaction susceptibility and liquefaction potential can be used in planning to mitigate and/or reduce earthquake hazards. Since 1992, under the auspices of the Seismic Hazards Mapping Act of 1990, earth scientists of the California Geological Survey have been mapping liquefaction potential across the entire State, beginning in the Los Angeles and San Francisco Bay areas and subsequently working to extend this mapping statewide (California Geological Survey, 1997).

Past large earthquakes have triggered liquefaction-related ground failure in many areas of California, as summarized in Table A1-1.

Table A1-1. Documented Occurrences of Liquefaction in Some Previous Moderate and Large California Earthquakes

Earthquake	Observed Phenomena	References
1857 Fort Tejon (M_w 7.9)	Ground fissuring in the beds of the Los Angeles, San Gabriel, Santa Clara, and Santa Ana Rivers, and sand boils occurred at Santa Barbara and in the flood plain of the Santa Clara River.	Agnew and Sieh (1978)
1933 Long Beach (M_w 6.4)	Liquefaction-related damage in parts of Compton, Huntington Beach and Long Beach.	Barrows (1974), Tinsley and others (1985, fig. 127, p. 264)
1973 Point Mugu (M_w 5.3)	Ground failures due to liquefaction were noted in the coastal estuarine areas near Port Hueneme and along the lower reaches of Calleguas Creek.	Weber and Kiessling (1976)
1971 San Fernando (Sylmar) (M_w 6.6)	Liquefaction-related failures occurred in the Van Norman Dam area of the northern San Fernando Valley, the Juvenile Hall, Sylmar Converter Station and the Joseph Jensen Filtration Plant, and elsewhere	Youd (1971), Seed and others (1975)
1979 and 1981 Imperial Valley (M_w 6.9 and M_w 5.9	Liquefaction-induced ground failures caused extensive damage to roads, utilities, irrigation canals and other agricultural facilities.	Youd and Wieczorek (1982, 1984)
1989 Loma Prieta (M_w 6.9)	Observed liquefaction of fill deposits around the margin of San Francisco Bay that caused extensive damage to buildings and utilities, and widespread liquefaction of fluvial and estuarine sand deposits in the Pajaro and Salinas river valleys and the Monterey Bay lowland areas of Santa Cruz and Monterey Counties.	Tinsley and others (1998)

Earthquake	Observed Phenomena	References
1994 Northridge earthquake (M_w 6.7)	Liquefaction and soft clay ground failures occurred as far south as the Los Angeles and Long Beach harbors, and as far north as the Santa Clara River valley, including the Potrero Canyon and Van Norman reservoirs areas.	Holzer and others, (1999)
2003 San Simeon (M_w 6.6)	Liquefaction as lateral spreads and sand boils appeared along natural drainages several kilometers east of the epicenter. Directivity and site amplification of seismic waves caused lateral spreads and sand boils in eolian dunes and fluvial deposits in the Oro Grande-Oceano-Pismo Beach areas and damaged the beachside communities.	Holzer and others, (2005)

The occurrence of liquefaction during a specific earthquake is restricted chiefly to certain geologic and hydrologic settings that experience high levels of ground shaking. Directivity, a phenomenon that produces enhanced ground motion (and in particular long-period motions) ahead of a propagating rupture also appears to play a role in controlling both the occurrence and severity of liquefaction-related ground failures, as observed in the 1989 Loma Prieta, 1994 Northridge, and 2003 San Simeon earthquakes (Holzer, 1998; Holzer and others, 1999; Holzer and others, 2005). Liquefaction is generally restricted to water-saturated, cohesionless granular sediment occurring at depths of less than 50 feet.

Types of Liquefaction Ground Failure

Youd (1978a, 1978b) identified four types of ground failure commonly resulting from liquefaction. These are: 1) lateral spread, 2) ground oscillation, 3) loss of bearing strength, and 4) flow failure. Flow failures, or soil flows, are restricted to slopes of greater than 3°. This ground failure mechanism is covered in more detail in the subsequent discussion of earthquake-induced landslides.

A “lateral spread” ground failure describes the case where lateral displacement of surficial blocks of sediment occurs due to liquefaction that develops in a subsurface layer. Once the process of liquefaction transforms one or more subsurface layers into a fluidized mass, gravitational forces plus inertial forces resulting from the earthquake’s ground motions may cause the mass to move down slope or toward a free face, such as a cut slope or incised river channel. Historically, lateral spreads occur on gentle slopes that range from about 0.3° to 3°. Amounts of horizontal displacement range from millimeters to several meters and appreciable differential settlement may also occur between displaced blocks. Greater horizontal and vertical displacements occur where (a) the liquefied layer is relatively thick, (b) the boundary conditions are favorable for lateral displacement, as when the location is near a free face, (c) the soil is especially loose or otherwise susceptible to liquefaction, (d) where the earthquake shaking is of greater duration, or e) where the depth to ground water is particularly shallow. Lateral spreads are especially destructive to pipelines, roads, utilities, bridge piers, or structures with shallow foundations. Figures A1-9 and A1-10 show typical lateral spreads developed in late Holocene deposits from the M_w 1989 Loma Prieta earthquake.

Figure A1-9. Liquefaction-induced lateral spread ground failure resulting from the M_w 6.9 1989 Loma Prieta earthquake destroyed a model airplane runway along the lower Pajaro River, Santa Cruz County, California. Extensional fractures formed separating blocks of less deformed late Holocene alluvium as blocks moved laterally a total of 9.8 meters towards the free face represented by the river's channel (Tinsley and others, 1998). Photograph by John Tinsley, U. S. Geological Survey.

Figure A1-10. Arcuate low scarps (shadowed) and a graben mark the headscarp of a liquefaction-induced lateral spread ground failure produced by the M_w 1989 Loma Prieta earthquake trends across a fallow strawberry field east of the unincorporated town of Pajaro, Monterey County, California. Extensional movement from left to right was towards the Pajaro River. Vertical settlements amounting to several tens of centimeters also developed along some of the fractures.

Ground oscillation takes place where liquefaction occurs at depth, but the slopes either are too gentle to permit lateral displacement, or there is no free-face to accommodate the lateral movement. During a liquefaction event, intact soil blocks that overlie the liquefied layer may decouple from each other and oscillate on the liquefied substrate. The resulting ground oscillation may be observed as traveling ground waves. There is typically little net displacement, but the ground may be cracked. Differential ground settlements sufficient to damage structures and sub-grade utilities may be observed especially where sufficient volumes of sand and water are vented to the ground surface from the liquefied substrate. These surface vents or "sand boils" (Figure A1-11) are commonly localized along fissures between blocks of intact soil (Youd and Perkins, 1978).

Figure A1-11. "Sand boils" composed of a liquefied mixture of sand and water erupted through fractures in the middle of a larger lateral spread caused by the 1989 Loma Prieta earthquake in Monterey County, California. Sand boils are the prima facie field evidence of liquefaction. Sand boils may be present in areas where lateral spreading is not expressed. Photograph by John C. Tinsley, U. S. Geological Survey.

Loss of bearing strength can occur beneath a structure when the subjacent soil loses shear strength, progressively weakening as it liquefies. Large deformations can then occur within the liquefied soil mass that involves any overlying deposits or buildings. Among the most spectacular examples of this ground failure mode was the tilting of structures up to 60° in the Kwangishicho apartment complex at Niigata, Japan, a result of liquefaction caused by the 1964 Niigata earthquake (Figure A1-12). Along the Pajaro River during the 1989 Loma Prieta earthquake, extensive liquefaction in point bar and channel deposits fractured flood control levees as the overlying soil mass that included the levee sank differentially into the liquefied substrate (Figure A1-13). Buried structures that are buoyant may rise if the soil layers holding them in place lose strength through liquefaction. Underground fuel storage tanks, empty septic tanks or swimming pools have been known to float following liquefaction events.

Figure A1-12. Liquefaction-induced bearing-failure loss resulting from the M_w 7.5 1964 Niigata, Japan earthquake caused structures in the Kwangishicho apartment complex to tilt and collapse due to differential settlement of the ground. Approximately 1/3 of the city subsided as much as 2 meters as a result of sand compaction. Photo courtesy of the National Geophysical Data Center.

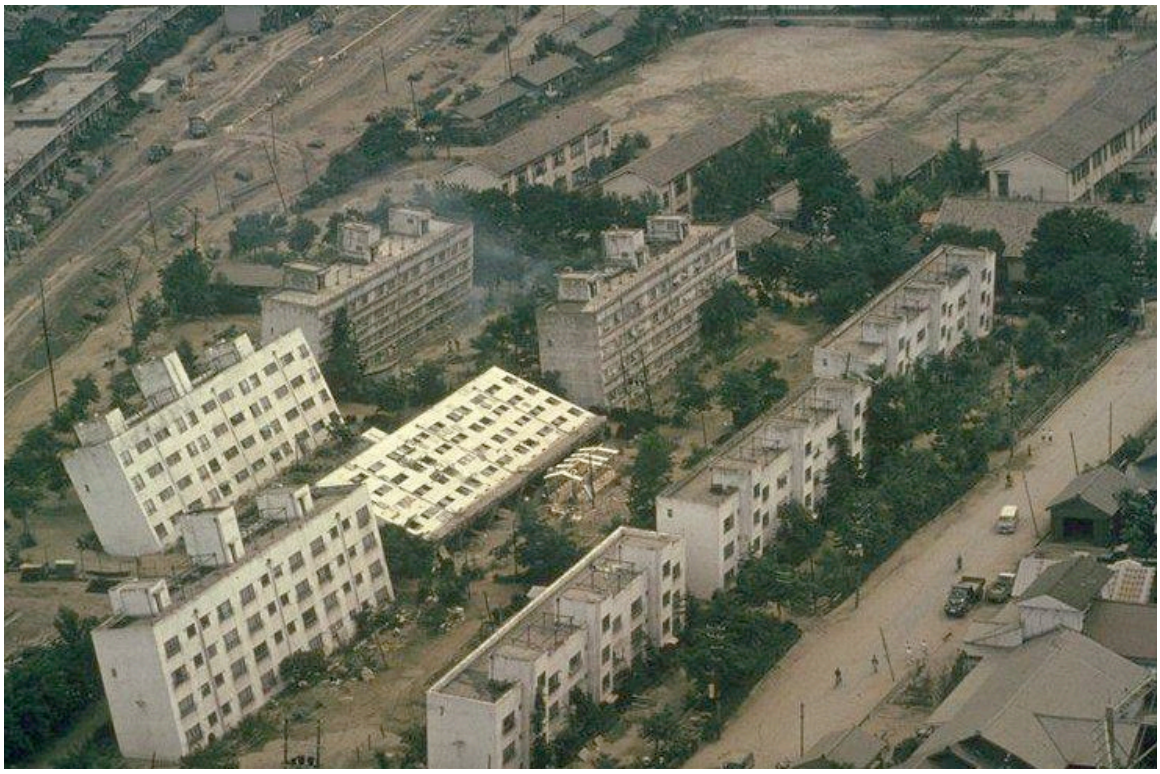

Figure A1-13. Liquefaction-induced bearing capacity failure of a flood control levee along the south bank of the lower Pajaro River, Monterey County, California, caused by the 1989 Loma Prieta earthquake. Earthquake shaking liquefied channel deposits of the river beneath the levee. The liquefied zone could no longer support the overlying ground, including the extra mass of the levee itself. The levee spread laterally (to the right of the photograph) towards the Pajaro River, opening the fractures that are highlighted by shadows along the sides of the levee embankment. Because of the additional weight, the highest parts of the levee sank further into the liquefied substrate than did the lower parts of the levee. Thus, the scarps that developed as a result of differential settlement of the levee's mass face away from the river and towards the axis of the levee. Photograph by John C. Tinsley, U. S. Geological Survey.

Ground deformation due to lateral spreading, and settlements from lateral spreading, ground oscillation, and loss of bearing strength are all expected to occur within the eight county study region as a result of the ShakeOut Scenario.

Controls on Liquefaction

Geologic and hydrologic factors that affect liquefaction susceptibility are 1) the age and type of sedimentary deposit, 2) the looseness of the sediment, especially cohesionless sediment, and 3) the depth to perched or regional ground water. Examining historical occurrences of liquefaction indicates that the more recently a deposit was formed, the looser it is and thus the easier it is to liquefy it. Moreover, certain types of deposits such as river channel and laterally-accreted flood-plain deposits are more susceptible to liquefaction than others, such as alluvial fan deposits (Youd and Perkins, 1978; Tinsley and Dupre, 1992). Sedimentary source factors (provenance) partly determine the nature of the Quaternary sediment in most basins. Sediment transport processes influence grain size, sorting and grading, and bedding characteristics of deposited sediment (Tinsley and others, 1985, p. 269).

The distribution of particle sizes (sorting or grading) and the grain-to-grain relations (packing) present in a deposit profoundly influence liquefaction susceptibility. Fine sand and silty sand are most easily liquefied, probably because these textural classes are still sufficiently loose to be able to have fairly high porosity, but small enough to limit permeability, which restricts the dissipation rate of any elevated pore fluid pressure that is generated as a result of seismic shaking. Gravelly sand, bouldery and cobbly gravel deposits, or deposits containing more than 15% clay are far less likely to liquefy. The coarser textured sediment allows pore fluid pressures to dissipate quickly and clayey deposits tend to be too cohesive to liquefy.

Because they are generally less dense, youngest Holocene-age deposits (<1000 years old) are the most susceptible to liquefaction. Earlier Holocene-age deposits (>1000 – 10,000 years old) are less

susceptible to liquefaction, mainly due to ongoing weathering processes that render the sediment progressively denser with time. Over thousands of years, wind and rainfall introduce dust particles to the landscape and these the particles migrate down into the pores between grains of sediment. This progressive infilling of fine particles increases a deposit's density, and alters the water-holding capacity of the soil layer at the surface. Once water can be retained within the soil mass, rock fragments and mineral grains, feldspar for example, undergo hydrolytic weathering to produce clay minerals in situ. As the build-up of clay progresses, the soil mass eventually becomes immune to liquefaction due to an increase in cohesion in what once was a cohesionless deposit. Earthquakes that shake the area may also serve to help densify the soil over time. Geologists refer to these subtle changes in a sedimentary deposit as "diagenesis" and understand that diagenesis alters the susceptibility of sediment to liquefaction.

Pleistocene deposits (>10,000 – 1.6 million years old) typically have clay-rich soil profiles that are much thicker than Holocene soil profiles and are correspondingly less susceptible to liquefaction. Therefore, as a result of their generally advanced states of diagenesis and weathering, Pleistocene and older deposits in southern California are generally unlikely to liquefy during earthquakes, even when saturated with ground water. Moreover, many Pleistocene surficial deposits in southern California also tend to be deformed or uplifted by folding and/or faulting, which causes these deposits to be eroded and drained of any ground water that otherwise might help produce liquefaction during earthquakes.

Within the eight-county area impacted by the ShakeOut Scenario earthquake, surficial deposits susceptible to liquefaction and that contain shallow ground water occur within parts of the Santa Clara River /Oxnard Plain areas of Ventura County, the San Fernando and San Gabriel valleys, portions of the coastal basin or flatland areas of Los Angeles and Orange counties, the Santa Ana River corridor, Imperial Valley, the southern Coachella Valley, coastal areas of San Diego County, and within small drainages in mountainous regions. Liquefaction-induced lateral spreads and settlements can be anticipated in these regions where ground motions from the Scenario earthquake are sufficiently high, particularly near the San Andreas fault. The ShakeOut Scenario earthquake is capable of producing liquefaction-induced differential displacements that exceed 3 meters. As with surface faulting, buildings and other infrastructure exposed to liquefaction are likely to suffer extensive damage.

Earthquake-Induced Landslides

The number of landslides triggered and the geographic area affected by earthquake-induced landslides generally scale with the earthquake magnitude. Consequently, earthquake-triggered landslides are a major source of damage and can pose a significant hazard to the built environment. Studies of earthquake-induced landslides have been ongoing for about five decades. Keefer (1984) published a seminal paper addressing the classification and occurrence of earthquake-triggered landslides. Subsequent published findings mainly have confirmed the trends and conclusions he outlined on the basis of 40 earthquakes of magnitudes ranging from about M_w 5.3 to M_w 8.6, and the attendant earthquake-triggered ground failures that he analyzed.

Landslides are gravity-driven phenomena and thus are more likely to occur on steep slopes. Aside from slope and the intensity of ground shaking, a primary control on landslide occurrence is the strength of the earth material, which can also be reduced by the presence of ground water. Both rock and soil can be involved in landslides. Varnes (1978) defines rock as "hard or firm rock that was intact and in its natural place before the initiation of movement." He also defines "soil" as "any loose, unconsolidated, or poorly cemented aggregate of solid particles, generally of natural mineral, rock, or

inorganic composition" which includes weathered or loose rock, sand, silt, clay and gravel, as well as organic topsoil. In general, rock is less susceptible to failure than soil, with strongly cemented rocks (eg. crystalline rocks and well-cemented sandstone) generally having the highest shear strengths and are thus the least susceptible to failure. In contrast, clayey soils, argillaceous sediment, and existing landslide deposits tend to be the most susceptible to failure. Within a single rock type, however, such characteristics as the prevalence of joints or fractures, orientation of bedding surfaces with respect to slope, and ground water conditions can greatly affect the susceptibility of rock or soil to failure. Whether rock or soil or a combination of these two end-members, a landslide's constituent materials help to define and to classify the type of ground failure that can develop.

Keefer (1984) showed that the abundance of seismically triggered landslides varies directly with the magnitude of the earthquake. The smallest earthquake in Keefer's dataset, the 1957 M_w 5.3 Daly City, California, earthquake, produced just 23 landslides. In contrast, the largest earthquake he evaluated (the 1950 M_w 8.6 Assam, India, earthquake) triggered more than 100,000 slides. Based on Keefer's evaluations, we expect that the ShakeOut Scenario earthquake will likely trigger between 10,000 and 100,000 landslides.

As the number of landslides increases with earthquake magnitude, the size of the area that is affected by earthquake-triggered landslides also increases by roughly a factor of 10. Keefer and Wilson (1989) derived a regression equation to express this relation. For purposes of a quick comparison, a $M_w = 5$ earthquake would be expected to trigger landslides in an area of about 44 km^2, a $M = 6$ earthquake would affect 441 km^2, a $M_w = 7$ earthquake would affect 4410 km^2; a $M_w = 8$ earthquake would affect 44,100 km^2 and a $M_w = 9$ earthquake would cause landslides across some 441,000 km^2 (Figure A1-14).

Figure A1-14. As earthquake magnitude increases, so does the average area within which an earthquake is likely to trigger landslides (from Keefer and Wilson, 1989). Areas shown are designed to illustrate that large areas can be impacted by seismically-triggered landslides and that the impacted areas generally scale with magnitude. Local geology and slope, however, ultimately control the distribution of landslides within an impacted region.

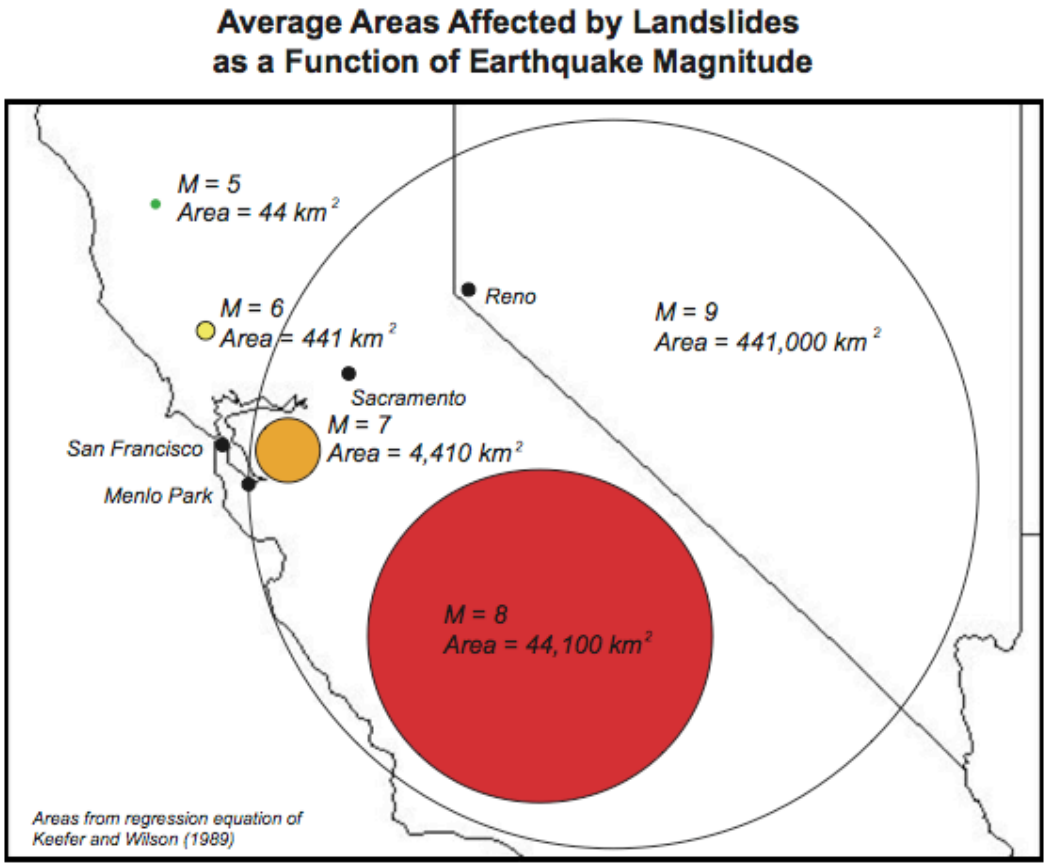

Types of Earthquake-Induced Landslides

Keefer (1984) recognizes three major categories of landslides and offers a 3-fold further subdivision of each of the three major categories according to the material and type of movement (Figure A1-15). The three major categories of earthquake-induced landslides are: Category 1 - disrupted slides and falls, Category 2 - coherent slides; and Category 3 - lateral spreads and flows.

Figure A1-15. Keefer's (1984) 3-fold classification of earthquake-induced landslides according to type of movement and major category of the failure (after Keefer, 1984).

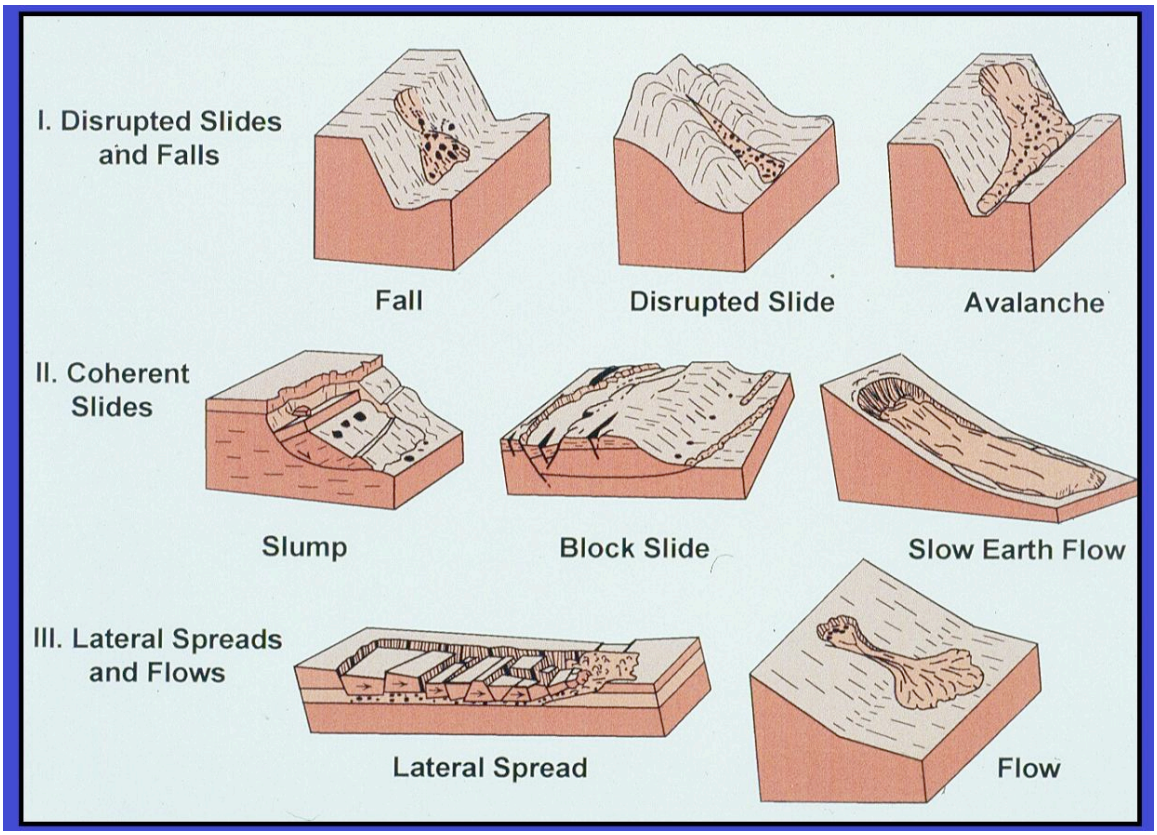

Category 1 landslides consist of highly disrupted slides and falls. These landslides include rock falls, rock slides, rock avalanches, soil falls, disrupted soil slides and soil avalanches. Perhaps the most distinguishing characteristic of this class of landslide is that the failed material occurs as highly disaggregated masses, small blocks, fragments or particles as distinct from more coherent landslide failures composed of much larger and more coherent blocks of earth material. Category 2 landslides are coherent landslides and include slumps, block slides and slow earth flows. These landslides generally are composed of comparatively large blocks of failed earth materials that are readily distinguished from the Category 1 landslides. Category 3 landslides include lateral spreads and flows that owe their mobilization to the onset of elevated pore fluid pressures induced by shear waves and surface waves in water-saturated susceptible subsurface layers. This type of ground failure includes liquefaction lateral spreads, which is covered in more detail in the previous section on liquefaction.

Category 1 landslides comprise about 80% of earthquake-triggered landslides worldwide in terms of relative abundance. Post-earthquake mapping of Category 1 landslides indicates that these landslides tend to occur mainly on steep slopes or precipitous terrain and are commonly observed to run out onto gentler slopes that lie below. These landslides tend to move at relatively high velocities and to travel for relatively large distances. With the exception of rock avalanches, these landslides tend to be thin or shallow-seated features, typically less than about 3 meters in thickness or depth to the failure surface. Because of the rapidity of movement and the long distances that material can travel, disrupted slides and falls composed of rock carry a moderate to high potential for producing human casualties, but a relatively low potential for producing casualties if composed of soil. On the basis of 40 historical earthquakes studied by Keefer (1984), disrupted slides and falls result in low to moderate loss to buildings and infrastructure, even though this category of slide is the most abundant produced by earthquakes worldwide.

Figures A1-16 through A1-18 illustrate different types of disrupted slides and falls commonly found following earthquakes. A noteworthy secondary hazard from disrupted slides and falls comprising Category 1 landslides is airborne disease. Many of these landslides commonly produce great quantities of dust. In the arid southwest, soils commonly contain the spores of *Coccidium sp*., the pathogenic fungus that causes Valley Fever (Coccidioidomycosis). If prevailing winds blow these pathogens across a populated area, susceptible individuals exposed to the pathogens may be taken ill by the disease. Following the 1994 Northridge, California, earthquake, numerous Category 1 landslides occurred in the Santa Susana Mountains and raised clouds of dust that were blown across the Simi Valley. Within eight weeks following the event, 203 cases of Valley Fever were reported (an order of magnitude greater that the expected number of cases) of which 3 were fatal. These deaths amounted to 4% of the total fatalities caused by the earthquake (Jibson and others, 1998; Jibson, 2002).

Figure A1-16. A building with its foundation undermined by a disrupted soil slide caused by the M_w 7.6 Chi-Chi, Taiwan, earthquake of 20 September 1999. The soil is composed of an aggregate of cobbles and finer grained particles; large intact blocks of failed earth materials, either rock or soil, are not present. Photograph by David Keefer, U. S. Geological Survey.

Figure A1-17. External and internal damage to an elementary school building caused by a rock fall triggered by the 3 July 1983 M_s 5.9 Costa Rica earthquake. *a).* One wall and a part of the roof were penetrated by falling rock. *b.)* A photograph taken inside the school building shows the large block of falling rock that opened the hole in the wall. Photograph by S. Mora (1983).

a)  b) 

Figure A1-18. Photograph of the Nevados Huascaran rock avalanche that was triggered by the 31 May 1970 M_w 7.9 Peruvian earthquake. This rock avalanche had an estimated volume of 50-100 million cubic meters. It traveled down slope through a distance of 16 km with a velocity of 280-335 km/hr and erased two villages, killing more than 18,000 persons. Photograph from Plafker and others (1971).

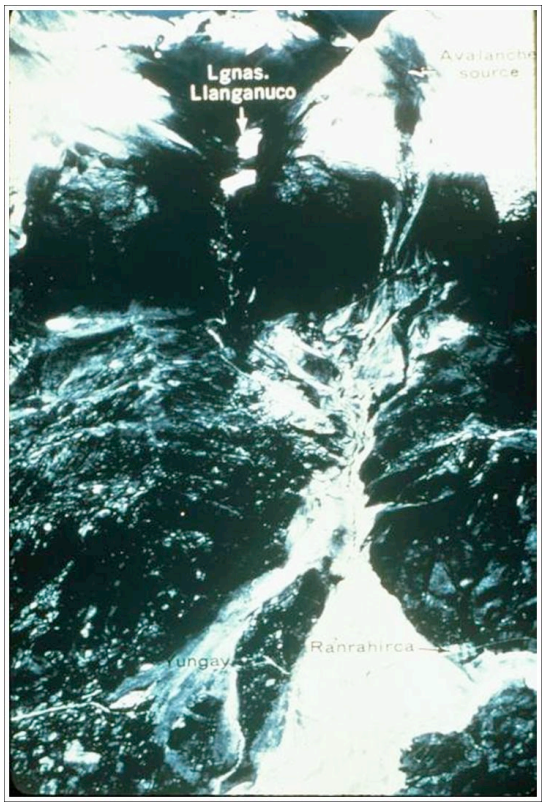

Category 2 landslides are coherent slides that are distinguished from disrupted slides and falls by being comprised of relatively coherent masses (one or a few large blocks). This category of landslides include soil slumps, soil block glides, rock slumps, rock block glides, and slow earth

flows; in terms of abundance, they represent about 12% of earthquake-triggered landslides. These types of failures tend to develop most commonly on moderate slopes and when they move, it is for comparatively short distances and with relatively low velocity compared to disrupted slides and rock falls. They tend to be rather deep-seated failures, generally exceeding 3 m in thickness or depth to the slide plane. Owing to the rather low displacement velocity and the characteristically short distances that they travel, coherent slides have a low to moderate casualty potential in rock, with a higher degree of casualty potential for soil. Historically, coherent slides cause moderate to high damage to structures and infrastructure, but low casualties (Keefer, 1984). Selected examples of coherent slides are shown in Figures A1-19 through A1-21.

Figure A1-19. Oblique aerial view showing a soil slump on a moderately steep grassy slope in the Santa Susana foothills of Los Angeles County, California, that was triggered by the 17 January 1994 Northridge, California, M_w 6.7 earthquake. The landslide mass is not disaggregated and has moved down slope towards the narrow stream valley that is partially in shadow in the foreground. Light-toned areas of bare rock and soil exposed by down-slope movement outline the slide mass. Photograph by David Keefer, U. S. Geological Survey.

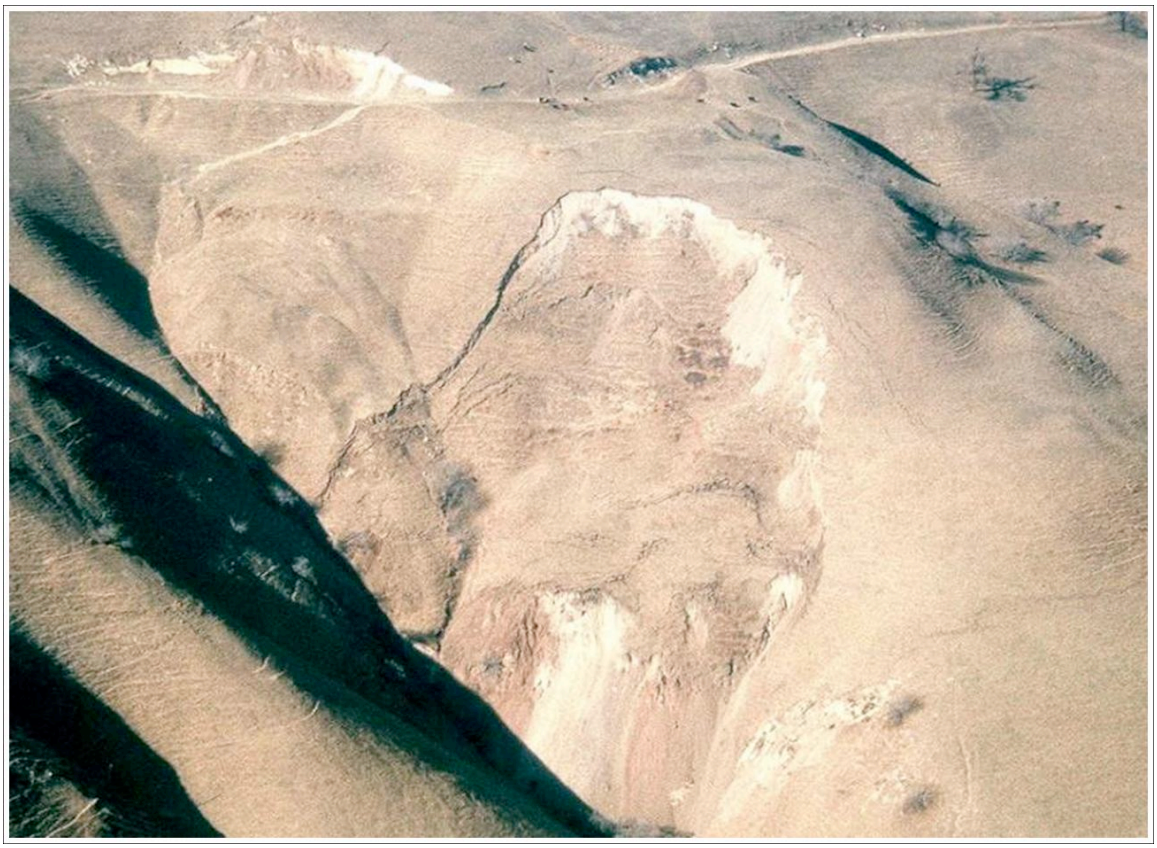

Figure A1-20. Oblique photograph showing the Government Hill landslide, a soil block slide that was triggered by the 28 March 1964, M_w 9.2, Anchorage, Alaska, earthquake. The relatively coherent slide mass destroyed several homes, paved roads, and other infrastructure. Individual blocks are indicated by the dark shadows cast along the margins of the blocks. Photograph from Hansen (1965).

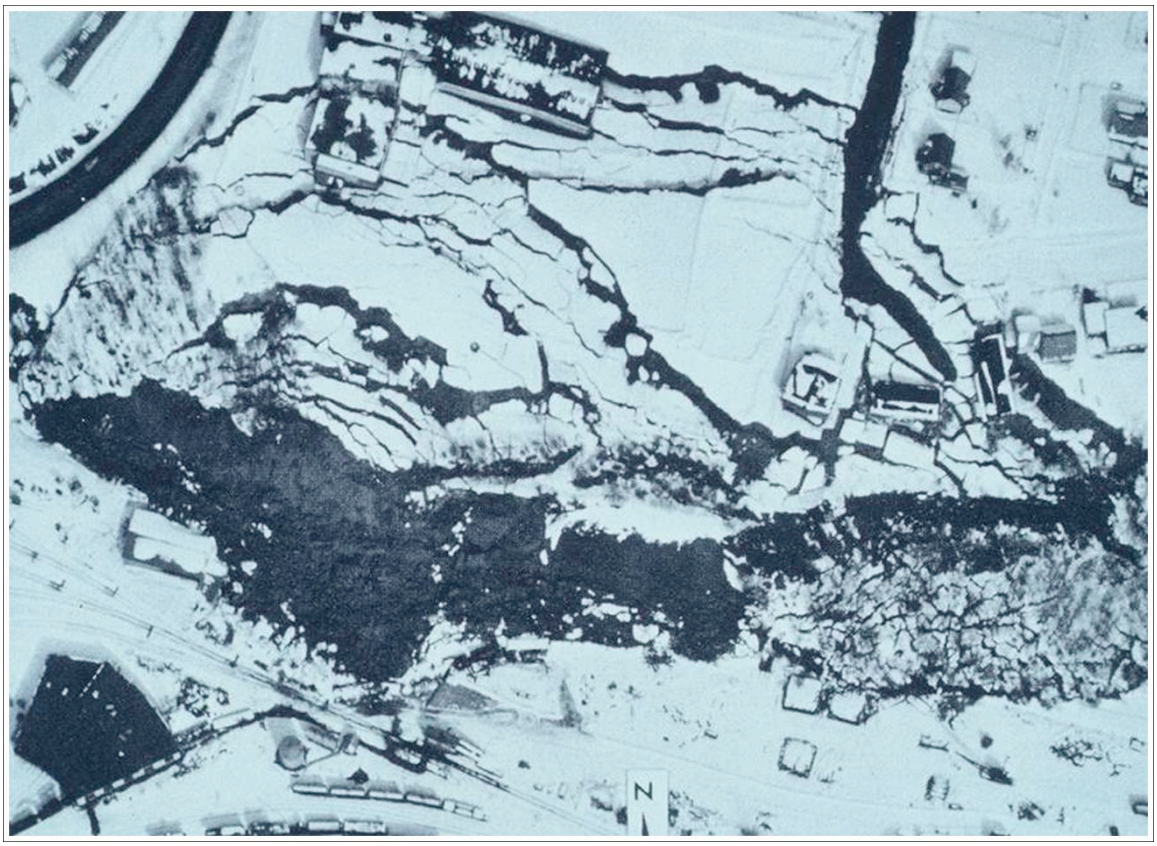

Figure A1-21. Photograph of a soil slump that developed in fill placed for a highway during construction. The slide was triggered by the 20 September 1999 M_w 7.6 Chi-Chi, Taiwan, earthquake. This type of landslide is quite commonly observed to affect roads and highways following moderate to great earthquakes worldwide. Photograph by David Keefer, U. S. Geological Survey.

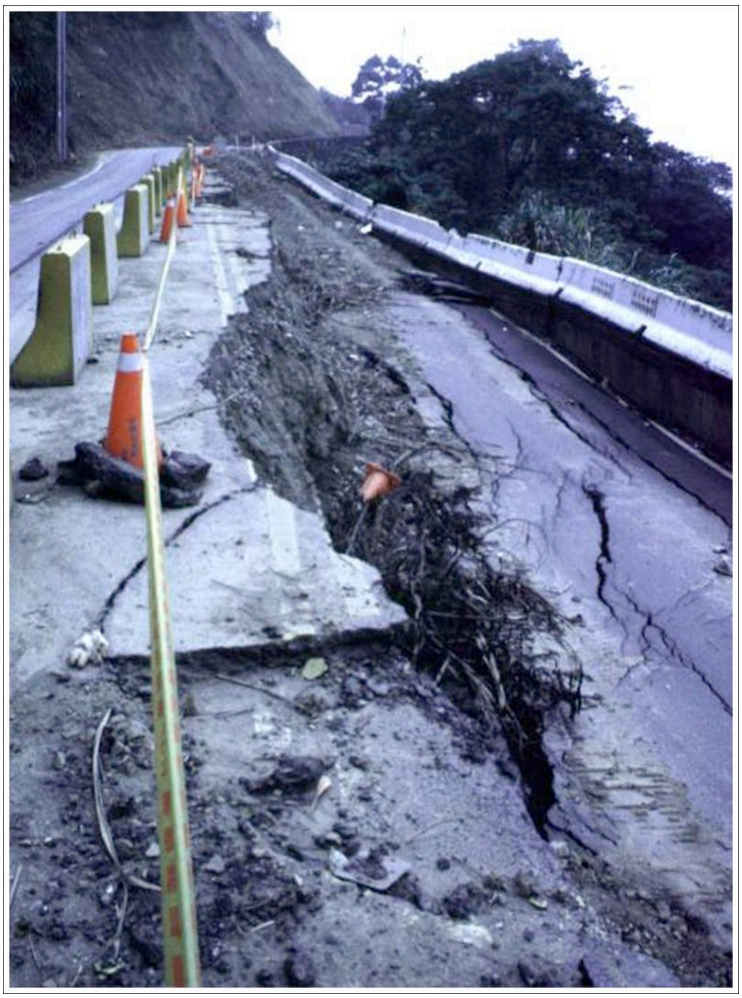

Category 3 landslides, or soil lateral spreads, rapid soil flows, and subaqueous landslides comprise roughly 8% of the total abundance of earthquake-triggered landslides. Lateral spreads, discussed previously, comprise more than 95% of this total category. The distinguishing characteristic of Category 3 landslides is that these failures involve liquefied soil masses (soil flows or flow failures) or discrete blocks moving on liquefied substrates (lateral spreads) that reflect the destabilizing influence of elevated pore fluid pressures. As such, these types of failures are generally considered to be liquefaction phenomena and are usually considered separately from other types of landslides. As discussed previously, lateral spreads characteristically occur on gentle slopes to nearly level ground, typically where a free face is available to accommodate lateral movement (see example, Figure A1-22). We expect that lateral spreads will be a common liquefaction failure produced by the ShakeOut Scenario event. Lateral spreads have a comparatively low casualty potential, owing to their low displacement velocity, but they can produce high levels of damage to buildings and subgrade utilities.

Soil flows develop on low to moderately steep slopes, typically exceeding 3°. Soil flows move at a comparatively higher velocity than soil slumps but slower than rock falls, and may travel over very large distances; they have been observed to transport material over distances of tens of kilometers and at velocities of several tens of kilometers per hour (Keefer, 1984; see example, Figure A1-23). Because of the high displacement velocities, soil flows are the most catastrophic of the liquefaction-related ground failures and have a high casualty potential. Fortunately, we do not expect soil flows to form from the ShakeOut scenario; conditions are too dry in this region to support catastrophic flow

failures, particularly in November, which is the time of year when the ShakeOut earthquake takes place.

Subaqueous landslides have been mapped offshore along the continental margin near Los Angeles (Gardner and Dartnell, 2002), and earthquakes could trigger additional subaqueous slides there. However, the expected ground motions from this event in the offshore area are too small to likely produce subaqueous slides, and we do not anticipate any occurring in this scenario (see Chapter 3E).

Figure A1-22. A lateral-spread type of ground failure that was triggered by the 23 January 2003 M_w 7.6 Colima, Mexico earthquake. The rows of pink paving stones have been disrupted and the balustrade toppled from movement of the more intact blocks that rode atop the liquefied substrate. The direction of displacement is away from the camera and toward the coastal lagoon, which represents an unconfined boundary condition (free face) for the lateral spread. Disrupted paving blocks show small settlements of several tens of centimeters. Photograph by David Keefer, U. S. Geological Survey.

Figure A1-23. A rapid soil flow, the Ontoke Kogen landslide, that was triggered by the 14 September 1984, Mw 6.2 Nagano-ken-seibu, Japan, earthquake. The elongated un-vegetated swath crossing the forested terrain from top to bottom shows that this landslide caused total devastation to anything that intercepted its lengthy path. Photograph by David Keefer, U. S. Geological Survey.

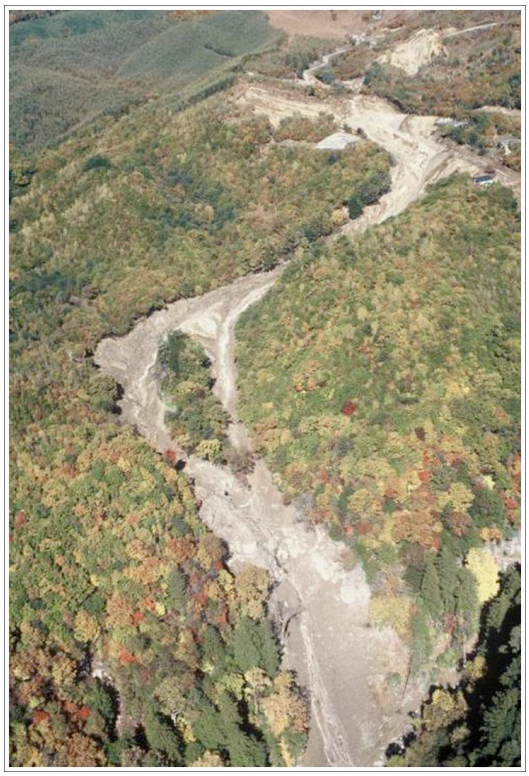

In addition to the principal landslide types described by Keefer (1984), ground fissures and differential displacements associated with ridge tops have been described from past earthquakes or have been postulated to have reactivated during earthquakes (Ponti and Wells, 1991; Hart and others, 1990; Plafker, 1967; Varnes and others, 1989). The origins of some shattered ridge tops and "ridge-top spreads" are controversial and may be controlled both by tectonics and gravitational forces. In any event, no methodology currently exists to predict the occurrence of these features. It is likely that ridge-top shattering and ridge-top spreading would be produced from the ShakeOut Scenario event, but the occurrences are likely limited and would result in little damage; therefore we have not considered these types of features in our analysis.

The ShakeOut Scenario earthquake is of sufficient magnitude that we should expect it to produce between 10,000 and 100,000 individual landslides. Of these, the vast majority will likely be Category 1 landslides, or highly disrupted slides and falls. Because many of these slides will occur on very steep slopes in relatively undeveloped mountainous areas, damage to buildings will likely be limited, although these slides could produce significant casualties to persons unfortunate enough to find themselves downslope from these failures. Damage or disruption to lifelines is likely where roads, railways, pipelines, etc. cross mountainous terrain. Within the eight-county area impacted by the ShakeOut Scenario earthquake, areas most susceptible to landsliding occur in portions of the Transverse Ranges of Ventura County and westernmost Los Angeles County, the eastern San Gabriel Mountains, the Puente Hills, and the northern Santa Monica Mountains; smaller pockets of high susceptibility areas also occur elsewhere in the region. Earthquake ground motions will be highest, however, in the eastern San Gabriel Mountains, so we anticipate that the greatest impacts from landsliding will occur there.

References

Acharya, H. K., 1997, Influence of fault bends on ruptures: Bulletin of the Seismological Society of America, v. 87, no., p.1691-1696.

Agnew, D. C., and Sieh, K. E., 1978, A documentary study of the felt effects of the great California earthquake of 1857: Bulletin of the Seismological Society of America, v. 68, p. 1717-1729.

Barrows, A. G., 1974, A review of the geology and earthquake history of the Newport-Inglewood structural zone, southern California: California Division of Mines and Geology Special Report 114, 115 p.

Barrows, A.G., Kahle, J.E., and Beeby, D.J., 1985, Earthquake hazards and tectonic history of the San Andreas Fault Zone, Los Angeles County, California: California Division of Mines and Geology Open-File Report 85-10 LA, 139p., maps 1:12,000.

Bryant, W. A. (compiler), 2005, Digital Database of Quaternary and Younger Faults from the Fault Activity Map of California, version 2.0: *http://www.consrv.ca.gov/CGS/information/publications/QuaternaryFaults_ver2.htm*

California Department of Conservation, Division of Mines and Geology, 1997, Probabilistic seismic hazard assessment for the State of California: California Division of Mines and Geology Open-File Report 96-08, 60 p., including appendices.

California Geological Survey, 1997, Guidelines for evaluating and mitigating seismic hazards in California: California Geological Survey (California Division of Mines and Geology) Special Publication 117, 74 p.

California Geological Survey, 2002a, Seismic Hazard Zone Report for the Camarillo 7.5-Minute Quadrangle, Ventura County, California,: California Geological Survey Seismic Hazard Zone Report 054, 45 p.

California Geological Survey, 2002b, Seismic Hazard Zone Report for the Ojai 7.5-Minute Quadrangle, Ventura County, California,: California Geological Survey Seismic Hazard Zone Report 072, 51 p.

California Geological Survey, 2002c, Seismic Hazard Zone Report for the Oxnard 7.5-Minute Quadrangle, Ventura County, California,: California Geological Survey Seismic Hazard Zone Report 052, 27 p.

California Geological Survey, 2002d, Seismic Hazard Zone Report for the Pitas Point 7.5-Minute Quadrangle, Ventura County, California,: California Geological Survey Seismic Hazard Zone Report 073, 47 p.

California Geological Survey, 2002e, Seismic Hazard Zone Report for the Point Mugu 7.5-Minute Quadrangle, Ventura County, California,: California Geological Survey Seismic Hazard Zone Report 057, 45 p.

California Geological Survey, 2002f, Seismic Hazard Zone Report for the Santa Paula 7.5-Minute Quadrangle, Ventura County, California,: California Geological Survey Seismic Hazard Zone Report 061, 53 p.

California Geological Survey, 2003a, Seismic Hazard Zone Report for the Hi Vista 7.5-Minute Quadrangle, Los Angeles County, California,: California Geological Survey Seismic Hazard Zone Report 087, 29 p.

California Geological Survey, 2003b, Seismic Hazard Zone Report for the Lake Hughes 7.5-Minute Quadrangle, Los Angeles County, California,: California Geological Survey Seismic Hazard Zone Report 103, 49 p.

California Geological Survey, 2003c, Seismic Hazard Zone Report for the Littlerock 7.5-Minute Quadrangle, Los Angeles County, California,: California Geological Survey Seismic Hazard Zone Report 099, 45 p.

California Geological Survey, 2003d, Seismic Hazard Zone Report for the Matilija 7.5-Minute Quadrangle, Ventura County, California,: California Geological Survey Seismic Hazard Zone Report 064, 51 p.

California Geological Survey, 2003e, Seismic Hazard Zone Report for the Palmdale 7.5-Minute Quadrangle, Los Angeles County, California,: California Geological Survey Seismic Hazard Zone Report 105, 51 p.

California Geological Survey, 2003f, Seismic Hazard Zone Report for the Ritter Ridge 7.5-Minute Quadrangle, Los Angeles County, California,: California Geological Survey Seismic Hazard Zone Report 083, 53 p.

California Geological Survey, 2003g, Seismic Hazard Zone Report for the Santa Paula Peak 7.5-Minute Quadrangle, Ventura County, California,: California Geological Survey Seismic Hazard Zone Report 075, 51 p.

California Geological Survey, 2003h, Seismic Hazard Zone Report for the Saticoy 7.5-Minute Quadrangle, Ventura County, California,: California Geological Survey Seismic Hazard Zone Report 066, 49 p.

California Geological Survey, 2003i, Seismic Hazard Zone Report for the Sleepy Valley 7.5-Minute Quadrangle, Los Angeles County, California,: California Geological Survey Seismic Hazard Zone Report 106, 47 p.

California Geological Survey, 2003j, Seismic Hazard Zone Report for the Ventura 7.5-Minute Quadrangle, Ventura County, California,: California Geological Survey Seismic Hazard Zone Report 067, 53 p.

California Geological Survey, 2003k, Seismic Hazard Zone Report for the Whitaker Peak 7.5-Minute Quadrangle, Los Angeles County, California,: California Geological Survey Seismic Hazard Zone Report 077, 47 p.

California Geological Survey, 2004, Seismic Hazard Zone Report for the Lovejoy Buttes 7.5-Minute Quadrangle, Los Angeles County, California,: California Geological Survey Seismic Hazard Zone Report 086, 43 p.

California Geological Survey, 2005a, Seismic Hazard Zone Report for the Alpine Buttes 7.5-Minute Quadrangle, Los Angeles County, California,: California Geological Survey Seismic Hazard Zone Report 092, 29 p.

California Geological Survey, 2005b, Seismic Hazard Zone Report for the Del Sur 7.5-Minute Quadrangle, Los Angeles County, California,: California Geological Survey Seismic Hazard Zone Report 101, 49 p.

California Geological Survey, 2005c, Seismic Hazard Zone Report for the Little Buttes 7.5-Minute Quadrangle, Los Angeles County, California,: California Geological Survey Seismic Hazard Zone Report 089, 17 p.

California Geological Survey, 2005d, Seismic Hazard Zone Report for the Lancaster East 7.5-Minute Quadrangle, Los Angeles County, California,: California Geological Survey Seismic Hazard Zone Report 094, 33 p.

California Geological Survey, 2005e, Seismic Hazard Zone Report for the Lancaster West 7.5-Minute Quadrangle, Los Angeles County, California,: California Geological Survey Seismic Hazard Zone Report 095, 45 p.

California Geological Survey, 2005f, Seismic Hazard Zone Report for the Rosamond 7.5-Minute Quadrangle, Los Angeles County, California,: California Geological Survey Seismic Hazard Zone Report 093, 33 p.

Campbell, K.W. and Bozorgnia, Y., 2008, NGA ground motion model for the geometric mean horizontal component of PGA, PGV, PGD, and 5%-damped linear elastic response spectra for periods ranging from 0.01 to 10 s, *Earthquake Spectra*, **24**, in press.

Gardner, J. V., and Dartnell, P., 2002, Multibeam mapping of the Los Angeles, California Margin: U.S. Geological Survey Open-File Report 02-162, *http://geopubs.wr.usgs.gov/open-file/of02-162/.*

Hansen, W. R., 1965, Effects of the earthquake of March 27, 1964 at Anchorage, Alaska: U. S. Geological Survey Professional Paper 542-A, 68 p.

Hart, E. W., Bryant, W. A., Wills, C. J., and Treiman, J. A., 1990, The search for fault rupture and significance of ridgetop fissures, Santa Cruz Mountains, California, in The Loma Prieta (Santa Cruz Mountains), California Earthquake of 17 October, 1989, S. R. McNutt and R. H. Sydnor (Editors), California Division of Mines and Geology Special Publication 104, p. 83-94.

Holzer, T. L. ed., 1998, The Loma Prieta, California, earthquake of October 17, 1989 – Liquefaction: U. S. Geological Survey Professional Paper 1551-B, 314 p.

Holzer, T. L. and Youd, T. L., 2007, Liquefaction, ground oscillation and soil deformation at the Wildlife Array, California: Bulletin of the Seismological Society of America, v. 97, p. 961-976.

Holzer, T. L., Bennett, M. J., Noce, T. E., Padovani, A. C., and Tinsley, J. C., III, 2006, Liquefaction Hazard Mapping with LPI in the greater Oakland, California, area: Earthquake Spectra, v. 22, no. 3, 693-708 p.

Holzer, T. L., Bennett, M. J., Ponti, D. J., and Tinsley, J. C., III, 1999, Liquefaction and soil failure during 1994 Northridge earthquake: Journal of Geotechnical and Environmental Engineering, v. 125, No. 6, p. 438-452.

Holzer, T. L., Noce, T. E., Bennett, M. J., Tinsley, J. C., III, and Rosenberg, L. I., 2005, Liquefaction at Oceano, California, during the 2003 San Simeon Earthquake: Bulletin of the Seismological Society of America, Vol. 95, No. 6, p 1-16.

Jibson, R. W., 2002, A public health issue related to collateral seismic hazards: The valley fever outbreak triggered by the 1994 Northridge, California earthquake: Surveys in Geophysics, v. 23, n. 6, p. 511-528.

Jibson, R. W., Harp, E. L., Schneider, E., Hajjeh, R. A., and Spiegel, R. A., 1998, An outbreak of coccidioidomycosis (valley fever) caused by landslides triggered by the Northridge, California, earthquake: Geological Society of America, Reviews in Engineering Geology, v. 12, pp. 53-61.

Johnson, C. E., Rojahn, Christopher, and Sharp, R. V., 1982, The Imperial Valley, California, earthquake of October 15, 1979: U. S. Geological Survey Professional Paper 1254, 451 pp.

Keefer, D. K., 1984, Landslides caused by earthquakes: Geological Society of America Bulletin, Vol. 95, no. 4, pp. 406-421. Apr. 1984.

Keefer, D. K. and Wilson, R. C., 1989, Predicting earthquake-induced landslides, with emphasis on arid and semi-arid environments *in* Sadler, P. M. and Morton, D. M., eds., Landslides in a semi-arid environment, with emphasis on the inland valleys of southern California: Publications of the Inland Geological Society, vol.2, p.118-149.

Molnar, P., 1988, Continental tectonics in the aftermath of plate tectonics: Nature, v. 335, p. 131-137.

Morton, D.M., and Miller, F.K., 2003, Preliminary geologic map of the San Bernardino 30'x60' quadrangle, California: U.S. Geological Survey Open-File Report 03-293. *http://pubs.usgs.gov/of/2003/of03-293/*

Morton, D.M. and Miller, F.K., 2006, Geologic map of the San Bernardino and Santa Ana 30' x 60' quadrangles, California: U.S. Geological Survey, Open-File Report OF-2006-1217, scale 1:100000.

Plafker, G., 1967, Surface faults on Montague Island associated with the 1964 Alaska earthquake: U.S. Geological Survey Professional Paper 1045, 42 pp.

Plafker, George, Ericksen, G. E., and Fernandez, Concha, 1971, Geological aspects of the May 31, 1970, Peru earthquake: Seismological Society of America Bulletin, v. 61, no. 3, p. 543-578.

Ponti, D.J., and Wells, R.E., 1991, Off-fault ground ruptures in the Santa Cruz Mountains, California: Ridge-top spreading versus tectonic extension during the 1989 Loma Prieta earthquake: Bulletin of the Seismological Society of America, v. 81, n. 5, p. 1480-1510.

Roth, R.A., and Kavazanjian, E. Jr., 1984, Liquefactions susceptibility mapping for San Francisco, California: Bulletin of the Association of Engineering Geologists, v. 21, n. 4, p. 459-478.

Rymer, M.J., Boatwright, J., Seekins, L.C., Yule, J.D., and Liu, J., 2002, Triggered surface slips in the Salton Trough associated with the 1999 Hector Mine, California, earthquake: Bulletin of the Seismological Society of America, v. 92, n. 4, p. 1300-1317.

Rymer, M. J., Tinsley, J. C., III, Treiman, J. A., Arrowsmith, J. Ramon, Clahan, K. B., Rosinski, A. M., Bryant, W. M., Snyder, A., Fuis, G. S., Toke, N. A. and Bawden, G. A., 2006, Surface slip associated with the 2004 Parkfield, California, earthquake: Bulletin of the Seismological Society of America, Vol. 96, No. 4B, p. S11-S27.

Seed, H. B. and Alonso, J-L., 1973, Effects of soil-saturated interaction in the Caracas earthquake of 1967, in Earthquake engineering research at Berkeley: Berkeley, Calif., Report 72-23, University of California, College of Engineering Earthquake Engineering Research Center, p. 47-50.

Seed, H. B. and Idriss, I. M., 1967, Analysis of soil liquefaction: Niigata earthquake: Proceedings of the American Society of Civil Engineers, Journal of the Soil Mechanics and Foundations Division, v. 97, no. SM9, p. 83-108.

Seed, H. B., Lee, K. L., Idriss, I. M., and Makdisi, F. I., 1975, The slides in the San Fernando Dams during the earthquake of February 9, 1971: Proceedings of the American Society of Civil Engineers, Journal of the Geotechnical Engineering Division, v. 101, no. GT7, p. 651-688.

Seed, H. B., Tokimatsu, K., Harder, L. F., and Chung, R. M., 1985, Influence of SPT Procedures in Soil Liquefaction Resistance Evaluations: Journal of Geotechnical Engineering, American Society of Civil Engineers, , v. 111, n. 12, p. 1425-1445.

Spotila, J. A., Niemi, N., Brady, R., House, M., and Buscher, J., 2007, Long-term continental deformation associated with transpressive plate motion: The San Andreas fault: Geology, v. 35, no. 11, p. 967-970.

Tinsley, J. C. and Dupre, W. R., 1992, Liquefaction hazard mapping, depositional facies, and lateral spreading ground failure in the Monterey Bay area, central California, in Hamada and O'Rourke, eds., 1992 Proceedings of Japan-U.S. Conference on earthquake resistant design of lifeline facilities and countermeasures for soil liquefaction, 4th, Honolulu, Hawaii, May 27-29, 1992, v. 1, p. 71-86.

Tinsley, J. C., Youd, T. L., Perkins, D. M., and Chen, A. T. F., Evaluating liquefaction potential, *in* Ziony, J. I., Editor, 1985, Evaluating earthquake hazards in the Los Angeles region: U. S. Geological Survey Professional Paper 1360, p. 263-315.

Tinsley, J. C., III, Egan, J. A., Kayen, R. E., Bennett, M. J., Kropp, A., and Holzer, T. L., 1998, Appendix: Maps and descriptions of liquefaction and associated effects *in* Holzer, T. L., ed., The

Loma Prieta, California, earthquake of October 17, 1989: U. S. Geological Survey Professional Paper 1551-B, p. B287-B314, including 3 plates.

Varnes, David J., 1978, Slope movement types and processes, in Schuster, R. L. and Krizek, R. J., eds., Landslides – analysis and control: National Academy of Sciences Transportation Research Board Special Report 176, p. 11-33.

Varnes, D. J., Radbruch-Hall, D. H. and Savage W. Z., 1989, Topographic and structural conditions in areas of gravitational spreading of ridges in the Western United States, U.S. Geological Survey Professional Paper 1496*,* 28 pp.

Weber, F. H., Jr., and Kiessling, E. W., 1976, General features of seismic hazards of Ventura County, California, in Seismic hazards study of Ventura County, California: California Division of Mines and Geology Open-File Report 76-5 LA, p. 8-218.

Youd, T. L., 1973, Liquefaction, flow, and associated ground failure: U.S. Geological Survey Circular 688, 12 p.

Youd, T. L., and Perkins, D. M., 1978, Mapping liquefaction-induced ground failure potential: Proceedings of the American Society of Civil Engineers, Journal of the Geotechnical Engineering Division, v. 104, no. GT4, p. 433-446.

Youd, T. L., 1978a, Major cause of earthquake damage is ground failure: Civil Engineering, v. 48, no. 4, p. 47-51.

Youd, T. L., 1978b, Mapping liquefaction-induced ground failure potential: Proceedings of the American Society of Civil Engineers: Journal of the Geotechnical Engineering Division, v. 104, no. GT4, p. 433-446.

Youd, T. L., and Wieczorek, G. F., 1982, Liquefaction and secondary ground failure, in The Imperial Valley, California, earthquake of October 15, 1979: U. S. Geological Survey Professional Paper 1254, p. 223-246.

Youd, T. L., and Wieczorek, G. F., 1984, Liquefaction during the 1981 and previous earthquakes near Westmorland, California: U. S. Geological Survey Professional Paper 941-A, p. A68-A74.